Soft Matter

Accepted Manuscript

ROYAL SOCIETY OF CHEMISTRY

www.rsc.org/softmatter

Tuning Polyelectrolyte Multilayer Structure by Exploiting Natural Variation in Fucoidan Chemistry

*Tracey T.M. Ho [1], Kristen E. Bremmell [2], Marta Krasowska [1], Damien N. Stringer [3], Benjamin Thierry [1], and David A. Beattie [1]**

[1] Ian Wark Research Institute, University of South Australia, Mawson Lakes Campus, Mawson Lakes, SA 5095

[2] School of Pharmacy and Medical Sciences, University of South Australia, City East Campus, North Terrace, Adelaide, SA 5000

[3] Marinova Pty Ltd, 249 Kennedy Drive, Cambridge, TAS 7170, Australia

* Corresponding author: David.Beattie@unisa.edu.au

ABSTRACT

Fucoidan is a sulfated polysaccharide that is extracted primarily from seaweed. The polymer contains a natural variation in chemistry based upon the species of seaweed from which it is extracted. We have used two different fucoidans from two different seaweed species (*Fucus vesiculosus* – FV; and *Undaria pinnatifida* – UP) as polyanions for the formation of polysaccharide-based polyelectrolyte multilayers (PEMs), to determine if the chemistry of different fucoidans can be chosen to fine-tune the structure of the polymer film. Partially acetylated chitosan was chosen as the polycation for the work, and the presented data illustrate the effect of secondary hydrogen bonding interactions on PEM build-up and properties. Ellipsometry and quartz crystal microbalance with dissipation monitoring (QCM-D) measurements performed during film build-up enabled detailed measurements of layer thickness, adsorbed mass, and the dynamics of the multilayer formation process. High quality atomic force microscopy (AFM) images revealed the differences in morphology of the PEMs formed from the two fucoidans, and allowed for a more direct layer thickness measurement. X-ray photoelectron spectroscopy (XPS) confirmed the chemistry of the films, and an indication of the altered interactions between chitosan and fucoidan with variation in fucoidan type, but also with layer number. Distinct differences were observed between multilayers formed with the two fucoidans, with those constructed using UP having thinner, denser, less hydrated layers than those constructed using FV. These differences are discussed in the context of their varied chemistry, primarily their difference in molecular weight and degree of acetylation.

Keywords: Fucoidan, chitosan, polyelectrolyte multilayer, ellipsometry, QCM-D, AFM

INTRODUCTION

Polyelectrolyte multilayers (PEMs) [1, 2] are the focus of an intense research effort to develop functional soft matter coatings for surfaces and capsules [3-6]. Polysaccharide-based PEMs are a specific sub-group of PEM films that have some specific advantages for biomaterials applications [7]. They have been extensively studied for potential use in a range of applications, including controlled release of bioactive molecules [4, 8], lubrication coatings [9-11], and for controlled protein [12] and cell [13, 14] attachment. Chitosan [15] is the most commonly used polycation for such systems, with hyaluronic acid being the most commonly studied polyanion. However, there is much more variation in the choice of polyanion for polysaccharide-based PEMs, and many other polysaccharide polyanions have been used to form PEMs with chitosan (e.g. such alginate [16, 17], heparin [18], carboxymethyl cellulose [19], and dextran sulfate [20]).

The utility of these polymer films relies on being able to control the properties and structure of the multilayer. For a given polyanion-polycation pair, it is possible to obtain very different layer thicknesses, water content, and stability, by altering the formation conditions used to create the multilayer (i.e. salt concentration, counter ion identity, and pH) [21-25]. Often these variations are caused by altering the balance in the inter-polymer interactions, with solution conditions altering the relative contributions of ion-pairing [26, 27] (the primary interaction) and other secondary binding interactions, such as hydrogen bonding [28, 29] and hydrophobic interactions [30, 31].

Another way to alter the balance of primary and secondary interactions in polyelectrolyte multilayer growth (and thus gain fine control over final multilayer structure) is to use starting materials of subtly different chemical composition. Altering the degree and nature of chemical substitution using synthetic routes (common with cellulose-based polymers [32], and with chitosan [33]) is one methodology to obtain tailored properties. However, with some plant-based polysaccharide polyelectrolytes, it may be possible to rely on natural chemical variation of polymers extracted from different species of plant to produce multilayers with specific tailored characteristics.

In this study, we have chosen to use fucoidan as the polyanion partner for chitosan, to perform a comprehensive study of PEM structure, as a function of variation in fucoidan chemistry. Fucoidan is a sulfated polysaccharide derived mostly from marine plant sources, such as brown algae (seaweed) and marine echinoderms, like sea urchins and sea cucumber [34, 35]. Fucoidans are strong polyelectrolytes (pKa between 1.0 - 2.5 [36]) and have additional properties that make them ideal as soft matter coatings for biomaterials applications. They are antibacterial, antiviral, resistant to degradation by mammalian enzymes, and are anti-fouling [37, 38 39].

Fucoidan polymers also have an altered chemical structure depending on the algae from which they are extracted: different species of brown algae contain fucoidans with additional monosaccharides in the polymer, with the variations being predominantly in the concentration of galactose and xylose. Different species also contain varying levels of acetylation of the constituent sugars. These variations to carbohydrate composition and acetylation are known to influence their biological activity [37]. To determine whether these chemical variations can be used to tune the structure of PEMs, we have selected fucoidans extracted from two different seaweed species (*Fucus vesiculosus* (FV); and *Undaria pinnatifida* (UP)), and used them as the polyanion in fucoidan/chitosan PEM formation. FV fucoidan is a simple fucoidan with no acetylation, and a dominance of fucose in terms of its sugar composition; UP is a more complicated fucoidan with acetylation of the sugar monomers, and significant amounts of galactose in addition to fucose. Both polymers have a high degree of sulfation.

The study shows that variations in fucoidan chemistry significantly influence the characteristics of the PEMs, including layer thickness, hydration, and internal multilayer interactions. The results indicate that fucoidan/chitosan PEMs have the potential to be a flexible and versatile platform for soft matter surface treatments.

MATERIALS AND METHODS

Polymers, Solutions, and Substrates

Fucus vesiculosus fucoidan (FV) and *Undaria pinnatifida* fucoidan (UP) were supplied by Marinova Pty Ltd (Tasmania, Australia). Both samples are from the Maritech® range of fucoidan extracts. These are technical grade – and have purities of 93% (FV) and 96% (UP), with uronic acid being the major component in addition to the fucoidan. The structures of the two fucoidans are given in Figure 1, and the chemical composition and molecular weight distributions are given in Table 1 and Table 2. The peak molecular weight for FV is 117 kDa, and for UP is 68.3 kDa, although UP has significant amounts of high molecular weight material (see Table 2).

Chitosan (CH; high molecular weight, ≥ 75% de-acetylation, > 800 cP for 1 wt. % solution in 1% acetic acid) and polyethyleneimine (PEI; branched, 25,000 Da) were purchased from Sigma-Aldrich (Australia). Glacial acetic acid (AR) and potassium chloride (KCl, 99% AR) were purchased from Chem-Supply (Australia). KCl used for all solution preparation was calcined at 550°C for over 8 hours to remove any organic impurities, recrystallized, and then calcined at 550°C for over 8 hours again.

A stock solution of chitosan (10,000 ppm) was prepared in 0.1 M acetic acid and stirred overnight. The solution was then diluted to 500 ppm in 0.1 M KCl, and its pH was adjusted to 6 using small amounts of KOH (volumetric grade, Sharlau, Spain) prior to experiments. Solutions of *Fucus vesiculosus* and *Undaria pinnatifida* fucoidans (500ppm) were prepared in 0.1 M KCl and stirred overnight. PEI (500ppm) was prepared in 0.1 M KCl. FV and UP solutions were pH adjusted with KOH and HCl (volumetric grade, Sharlau, Spain) to pH 6 prior to experiments. All solutions were made with Milli-Q water of resistivity of 18.2 MΩ·cm, an interfacial tension of 72.4 $mN \cdot m^{-1}$ at 22 ºC, and a total organic carbon component of less than 4 $mg \cdot L^{-1}$. All fucoidan solutions were filtered using a 0.45 micron PTFE filter (Grace Davison Discovery Science, Australia), and all solutions were used within 24 hours from preparation.

Silicon wafers (p-type, <100>, Si-Mat Silicon Materials, Germany) were used for spectroscopic ellipsometry, atomic force microscopy (AFM), and X-ray photoelectron spectroscopy (XPS) experiments. Different silicon wafers (p-type, <100>, 25 mm in diameter, supplied by M. M. R. C. Pty Ltd, Australia), of custom size, were used for zeta potential determination. In both cases, the native oxide layer was of similar thickness (~ 2 nm). Prior to use, these were piranha (mixture of 3:1 H_2SO_4:30% H_2O_2) cleaned for 30 min followed by extensive rinsing in Milli-Q water, N_2 drying, and 60 s plasma clean (Harrick, USA). Silica-coated quartz crystal microbalance (QCM) crystals (QSX303, Q-Sense, Sweden) were immersed in 2% Hellmanex (Hellma Analytics, Germany) for 30 min, followed by extensive rinsing in Milli-Q water, N_2 drying and 60 s plasma cleaning prior to experiments. A different cleaning procedure was adopted for the QCM sensors as piranha cleaning can affect/remove the thin layer of sputtered SiO_2 on the sensors. The different cleaning methods are still effective in removing surface contamination, and will not affect/alter the zeta potential of the different substrates (see ESI).

Table 1: Chemical composition of the fucoidan polymers †.

	Carbohydrate (%)							Sulfate	Cation	Acetyl	Uronic Acid
	Total*	F	X	M	Ga	Gl	R	(%)	(%)	(%)	(%)
FV	58.7	44.5	7.1	2.7	3.1	1.3	0.0	28.4	6.0	0.0	4.9
UP	55.0	29.7	0.4	1.0	22.7	0.8	0.3	29.1	8.0	2.5	2.1

*Total carbohydrate (%) made up of: F – Fucose, X – Xylose, M – Mannose, Ga – Galactose, Gl - Glucose, and R – Rhamnose. † Information supplied by Marinova

Table 2: Molecular weight distribution of the fucoidan polymers †.

Percentage Within Mw Ranges (kDa)							
Fucoidan	% >1600	%1100-1600	%200-1100	% 60-200	%20-60	% 5-20	% <5
FV	2.4	2.8	34.7	31.4	15.2	4.7	8.8
UP	10.2	4.3	26.9	25.6	16.1	5.2	11.7

† Information supplied by Marinova

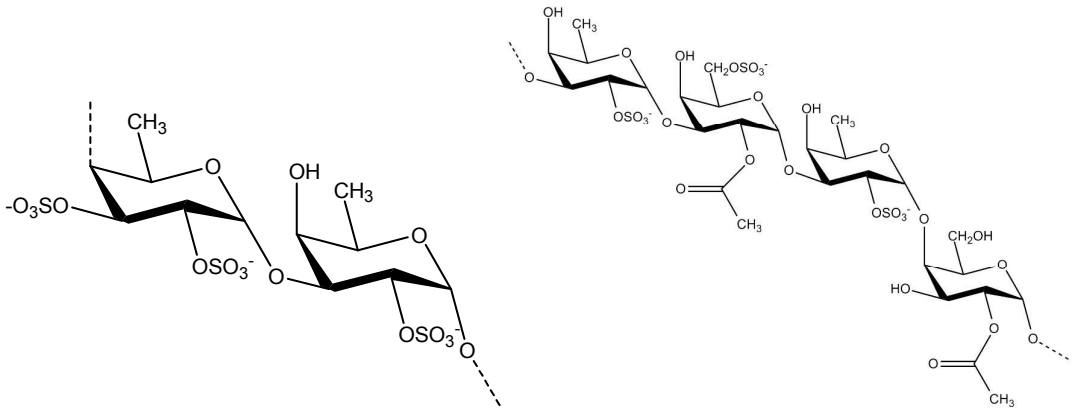

Figure 1: Schematic chemical structures of *Fucus vesiculosus* fucoidan (left – abbreviated to FV) and *Undaria pinnatifida* fucoidan (right – abbreviated to UP). Major structural differences include a small but significant amount of acetylation of sugar monomers in UP, and the presence of galactose in UP, in addition to fucose.

PEM Formation

Fucoidan/Chitosan multilayer build-up in all experiments involved: (i) initial adsorption of PEI for 15 min; (ii) 5 min rinse in 0.1 M KCl pH 6 (rinsing step); (iii) adsorption of fucoidan (FV or UP) for 15 min; (iv) a second 5 min rinsing step; (v) adsorption of chitosan for 15 min; (vi) a third 5 min rinsing step. Steps (iii) through to (vi) were repeated until the desired bilayer number was achieved. Both polymer solutions were at pH 6. At this pH, the fucoidans are likely to be fully charged (as mentioned above, they are strong polyelectrolytes, with a pKa between 1.0 - 2.5 [36]). The pKa of chitosan is approx. 6.5 [40], and it is likely that at pH 6 there will be a dominance of $-NH_3^+$ groups, but some $-NH_2$ groups will still be present on the chitosan chains.

The build-up of the multilayer was confirmed with zeta potential measurements, showing the characteristic charge reversal associated with the adsorption of oppositely charged polyelectrolytes [41, 42]. The zeta potential of PEM-coated silicon wafers was determined from streaming potential measurements using the spinning disc methodology [42] with a ZetaSpin 2.0 instrument (Zetametrix, USA). The measurement of zeta potential using the principle of rotating discs is well-known: [43] (i)

rotations of the sample induce the radial flow generated near the sample surface; (ii) the flow sweeps charge adjacent to the face of the sample towards the edge of the sample, producing spatially distributed streaming potential [44]. This measurement was performed in electrolyte of $1x10^{-3}$ M KCl, rather than the electrolyte concentration used during formation. This restriction was necessary as the adsorption solution is too high in ionic strength for any streaming potential instrument to operate reliably (due to compression of the electrical double layer for high salt concentrations). The zeta potential value for each stage of formation of the $(FV/CH)_{10}$ and $(UP/CH)_{10}$ multilayers is given in Figure S.1.

For XPS and AFM experiments, cleaned silicon wafers were first dipped into glass petri dishes containing the desired polyelectrolyte or rinsing solution. In quartz crystal microbalance with dissipation monitoring (QCM-D), the polyelectrolyte adsorption on silica coated quartz crystals was performed in the QCM chamber using a peristaltic pump (IPC-N4, Ismatec, USA) at a flow rate of 100 µl/min, followed by rinsing in 0.1 M KCl at pH 6 between each adsorption step, at a flow rate of 200 µl/min. Adsorption was carried out under flow to ensure that solution depletion of polymer from the small fluid cell volume did not affect the multilayer build-up.

For the adsorption of polyelectrolytes in ellipsometry, the polyelectrolyte solution was introduced into the ellipsometry liquid cell (5ml Vertical Liquid Cell, JA Woollam) using a peristaltic pump (flow rate 2 ml/min), followed by a rinse with 0.1 M KCl at pH 6 between each adsorption step (flow rate 15 ml/min). The volume of the liquid cell is much larger than the flow cell used in QCM-D, removing any concern about solution depletion affecting adsorption (which would be an issue if QCM-D experiments were not performed under flowing conditions). The larger flow rates (relative to the QCM) simply reflect the capacity/range of the peristaltic pump used for the experiments (experiments performed under static conditions yield approx. the same adsorption density).

All PEM formation experiments using the various techniques were repeated between three and ten times, using fresh polymer solutions and freshly prepared substrates. The data presented for all

techniques are representative datasets from the numerous experiments performed. Statistical analysis of these repeat measurements is given in the figures and along with the descriptions of the data for AFM and zeta potential measurements. For ellipsometry, the standard deviation of the final mass or thickness determined was approx. 5%; for QCM, the standard deviation in final adsorbed mass was approx. 15%.

Atomic Force Microscopy (AFM) Imaging

The *in situ* (i.e. hydrated in solution) morphology and thickness of the PEM films were determined from height AFM images acquired using the Multimode 8 (Bruker, USA) placed on an active anti-vibration table (Vision IsoStation, Newport, USA), and equipped with a vertical engagement scanner "J" (maximum scan range 125 μm in the x- and y-direction, and 5 μm in z-direction). The AFM images were collected in tapping and ScanAsyst modes in 0.1 M KCl at pH 6. In order to avoid any contamination, and to minimise the adsorption of polyelectrolytes on surfaces different than a silicon wafer, the quartz fluid cell was used without an O-ring. Even though the liquid surface area exposed to air was very small, care was taken to avoid any increase in salt concentration due to evaporation. A small amount (~ 0.15 ml) of 0.1 M KCl was added very carefully through the liquid cell inlet every 30 minutes (after every two AFM scans).

To acquire images in tapping mode silicon nitride cantilevers with a resonance frequency between 100 and 200 kHz, a spring constant between 0.35 and 1.40 N/m, and a sharp (nominal tip radius 2 nm) tip (NSL, Bruker, USA) were used. For imaging in ScanAsyst mode silicon nitride cantilevers with a resonance frequency between 40 and 75 kHz, a spring constant between 0.12 and 0.48 N/m, and a sharp silicon (nominal tip radius 2 nm) tip (SCANASYST-FLUID+, Bruker, USA) were used. All images were taken at high (512 x 512 or higher) resolution. Scan rates employed in imaging were 0.99 Hz or lower.

AFM images were also used to determine the thickness of the PEM films. The measurement of the height of PEM films was performed by first creating a scratch (using a scalpel blade) across the

film to expose the substrate (silicon wafer)[a]. Imaging the 'step' formed between the substrate results in height image, an example of which can be seen in Fig S.5 in the supporting information, along with a visible light microscope image of the cantilever above the step. Such images were analysed using WSxM 4.0 SPMAGE 09 Edition (Nanotec, Spain) [45] and NanoScope Analysis v 1.5 (Bruker, USA) software packages. The cross section of 'steps' was analysed in multiple locations to determine the height difference between the surface of the film and the bare substrate. AFM was also used to calculate peak-to-valley (PTV) and root mean square (R_{rms}) roughness. Scans were taken over 5 x 5 μm^2 area of the non-scratched PEMs. From these PTV and R_{rms} were calculated using the mentioned software packages. R_{rms} and PTV values are reported in the electronic supplementary information.

Spectroscopic Ellipsometry

Thickness measurements of *in situ* PEM film assembly on silicon wafers was performed using a J. A. Woollam vertical variable angle spectroscopic ellipsometer V-VASE (USA) equipped with a 5 mL vertical liquid cell (model TLC-100). The ellipsometric parameters, Ψ and Δ (amplitude ratio and phase difference of reflected p (r_p) and s (r_s) polarized light), were measured for the required range of wavelengths (400-1000 nm) at the angle of incidence close to 75°:

$$\tan(\Psi)\exp(i\Delta) = \rho = \frac{r_p}{r_s} \qquad (1)$$

Modelling and data analysis was performed using the WVASE32 software (JA Woollam, USA). A four layer model (Si/SiO_2/PEM/H2O ambient layer) was fitted to the experimental data. The optical properties of the silicon substrate, native oxide layer and H_2O ambient layer were taken from the library of the software. The thickness and refractive index of the PEM, n_{PEM} were obtained by

[a] To exclude the possibility of silicon wafer damage by the scalpel blade scratch (thus potentially affecting measured layer thickness), a clean silicon wafer was scratched with the scalpel blade and 5 x 5 μm AFM image was taken. The height images show no visible damage.

fitting the PEM layer as a single Cauchy medium (assuming the layer is a homogeneous transparent medium), with a refractive index defined by the following formula [46]:

$$n_{\mathrm{PEM}}(\lambda) = A_n + \frac{B_{\mathrm{n}}}{\lambda^2} + \frac{C_{\mathrm{n}}}{\lambda^4} \qquad (2)$$

The determined thickness and refractive index of the PEM are used to determine the adsorbed mass, using the de Feijter's equation[47]:

$$m_{\mathrm{opt}} = \frac{d_{\mathrm{opt}}\,(n_{\mathrm{PEM}} - n_{\mathrm{sol}})}{dn_{\mathrm{p}}/dc} \qquad (3)$$

where d_{opt} is the optical thickness determined by ellipsometry, n_{PEM} is the determined refractive index of the PEM, n_{sol} = 1.3324 is the refractive index of H_2O at 589 nm, and dn_p/dc (where c is the polymer concentration) = 0.155 cm^3/g is the refractive index increment for the polymer film. The value of dn/dc was chosen based on measurements of refractive index of solutions of chitosan and fucoidans, using a Multi-wavelength Abbe Refractometer (DR-M2, Atago, Japan). The value of dn_p/dc used in the calculation of adsorbed mass is the average of the two values determined for chitosan (approx. 0.18 cm^3/g) and for the fucoidans (approx. 0.13 cm^3/g).

Quartz Crystal Microbalance with Dissipation Monitoring (QCM-D)

The PEM build-up was monitored *in situ* by QCM-D (E4, Qsense, Sweden). The technique consists of a quartz crystal sandwiched between a pair of electrodes and is excited to oscillate through the application of an AC voltage. The measurements were performed on silica coated AT-cut 5MHz quartz crystals purchased from Q-sense, Sweden. QCM-D is a gravimetric technique that measures the changes in the resonance frequency (Δf) of the oscillating quartz crystal as molecules adsorb onto its surface. The change in dissipation energy (ΔD) is also measured simultaneously with Δf, providing information on the viscoelasticity of the adsorbed film [48]. ΔD is measured as the sensor is vibrated at its resonance frequency and is defined as:

$$D = \frac{E_{\mathrm{lost}}}{2\pi E_{\mathrm{stored}}} \qquad (4)$$

where E_{lost} is the dissipated energy during one oscillation cycle and E_{stored} is the total energy stored in the oscillator.

For a thin and rigid film, the decrease in frequency is related directly to the mass (Δm) of the adsorbed molecules, and can be calculated using the Sauerbrey relation [49]:

$$\Delta m = -\frac{C \cdot \Delta f}{n} \qquad (5)$$

where C = 17.7 ng Hz^{-1} cm^{-2} for a 5 MHz quartz crystal and n (= 3,5,7,9) is the overtone number. However, for adsorbed layers that are soft, the Sauerbrey relation becomes invalid. The limit of the validity of the Sauerbrey relation is commonly placed at the point where the ratio of $\Delta D/(-\Delta f_n/n)$ becomes greater than 4 x 10^{-7} Hz^{-1}. Below that value, the layer is deemed to be sufficiently rigid to validate the Sauerbrey relationship [50].

The viscoelastic properties of polyelectrolyte multilayers can be determined using the Voigt model [51], if one assumes that the film has a uniform thickness and uniform density. The Voigt model assumes that the adsorbed layer can be described as a slab of viscoelastic material with a complex, frequency-dependent shear modulus [18]:

$$G = G' + iG'' = \mu_f + i2\pi f \eta_f \qquad (6)$$

where η_f is the shear viscosity of the layer (the tendency to dissipate energy supplied to the film), otherwise termed the loss modulus; μ_f is the elastic modulus of the layer (a measure of the energy required to deform the layer by a given amount, and which will be returned after the application of force), otherwise termed the storage modulus. Both terms are related to the measured frequency and dissipation response of the adsorbed film [18, 50].

X-ray Photoelectron Spectroscopy

XPS experiments were performed on nitrogen dried PEM coated silicon wafers. PEM samples were rinsed briefly in Milli-Q water prior to nitrogen-drying, to prevent the formation of KCl crystals on the PEM surface. Measurements were made for 9.5- and 10-bilayer samples (9.5 has fucoidan as the outer layer; 10 has chitosan as the outer layer). In addition, XPS spectra were recorded for the bulk polymer powder samples (deposited on carbon tape, completely covering the

adhesive layer). The XPS measurements were recorded with an AXIS Ultra spectrometer (Kratos, UK) using a monochromatic Al Kα source ($h\nu$ = 1486.6 eV) operating at 15 kV and 10 mA. The pressure during analysis was 2 x 10^{-9} Torr. The spot size of analysis was approximately 300 μm x 700 μm. Survey spectra were collected over a range of 0-1120 eV binding energy with a pass energy of 160 eV and 0.5 eV step size. High resolution spectra were collected with a pass energy of 20 eV for C 1*s*, O 1*s* and N 1*s* with a 0.1 eV step size, and for S 2*p* with a 0.05 eV step size. All binding energies were calibrated using the aliphatic carbon at 285.0 eV. The XPS data was processed and peak-fitted using the CasaXPS software (including atomic surface concentrations), and Shirley backgrounds were used throughout [52].

RESULTS

Spectroscopic Ellipsometry

Spectroscopic ellipsometry has been used to determine the adsorbed mass, layer thickness, and optical constants of the multilayers at each stage of the build-up. These measurements were performed *in situ*, as the layer was building up, using a single-angle-of-incidence fluid cell assembly. The data presented in Figure 2 (top panel) is the determined layer thickness as a function of layer number (odd numbers = fucoidan; even numbers = chitosan) for both multilayer systems. Also given in the lower panel in Figure 2 is the refractive index (the 'A_n' parameter from the Cauchy layer – not wavelength dependent) for the multilayer system as a function of layer number (same odd/even ordering). Note: only values for layer numbers greater than 5 are given to ensure that the refractive index values are meaningful (i.e. for layers that are greater than a few 10s of nm thick). A full list of layer thickness and adsorbed mass (determined using the de Feijter equation) for each sample/layer number is given in the supporting information, in addition to the relevant Ψ and Δ versus wavelength plots for a full 10-bilayer multilayer (the raw data from which the instrument software determines the layer physical parameters). The final adsorbed mass values (m_{opt}) for the two multilayers are: $(FV/CH)_{10}$ = 10805 ng/cm^2; $(UP/CH)_{10}$ = 7779 ng/cm^2.

It should be noted that the ellipsometric thickness of a multilayer film is based on a number of assumptions. Ellipsometry makes an optical measurement of the sample, and the thickness is determined based on an assumed film structure (uniform thickness, uniform composition), using an optical model based on further assumptions. However, ellipsometry data is still valuable and presents a useful lens through which to view the formation of the multilayers. The thickness data for $(FV/CH)_{10}$ (filled triangles) illustrates that the multilayer growth is supra-linear, with a distinct increase in the thickness increment with bilayer number as the multilayer builds up, resulting in a layer thickness of 171 nm after 10 full bilayers have been added to the substrate. Supra-linear/exponential growth is seen often in multilayer formation, and is thought to be indicative of slightly less ordered layer build-up as the multilayer forms with higher bilayer numbers. The structural picture for this is normally one of interdigitation and interlayer penetration and migration of the adsorbing polymer [53].

The fine detail of the data, i.e. the measured thickness for each individual additional polymer layer, provides further insight into this deviation from the ideal picture of a stratified multilayer. It can be seen that the largest layer thickness increases are for the addition of the FV fucoidan (jumps of approx. 20 nm for each fucoidan adsorption after layer 11), with chitosan only adding smaller increments to the overall thickness (only 4-5 nm after layer 12). This could indicate only marginal adsorption of the chitosan at each stage, but the zeta potential data do not support this (see S1 in the supplementary information) – with significant positive charge obtained after each chitosan addition for every stage of the 10-bilayer build-up. It is most likely that there is a degree of densification/interdigitation/migration that occurs primarily upon the addition of the chitosan. This possibility is supported by the refractive index data – with the refractive index increasing significantly upon each chitosan layer addition, and decreasing upon each fucoidan addition. The layer becomes more optically (and thus physically) dense upon addition of each chitosan layer.

The data for $(UP/CH)_{10}$ is also given in Figure 2 (empty circles), with a final layer thickness of 104 nm being achieved after formation. As with $(FV/CH)_{10}$, the growth of the multilayer is non-

linear in terms of thickness versus layer number. However, the degree of non-linearity is reduced. In addition, the refractive index of the multilayer assembly is seen to be significantly higher than that calculated for $(FV/CH)_{10}$ at all layer numbers. This would indicate that the $(UP/CH)_{10}$ multilayer is more dense/less hydrated compared to the $(FV/CH)_{10}$ system. As with $(FV/CH)_{10}$, there is evidence of interdigitation/penetration of the chitosan into the multilayer assembly as the layer number reaches the second half of the formation (see lower panel of Figure 2). However, the variation in refractive index is slightly smaller for UP than for FV, indicating that there may be less interdigitation/migration in the case of the $(UP/CH)_{10}$ multilayer.

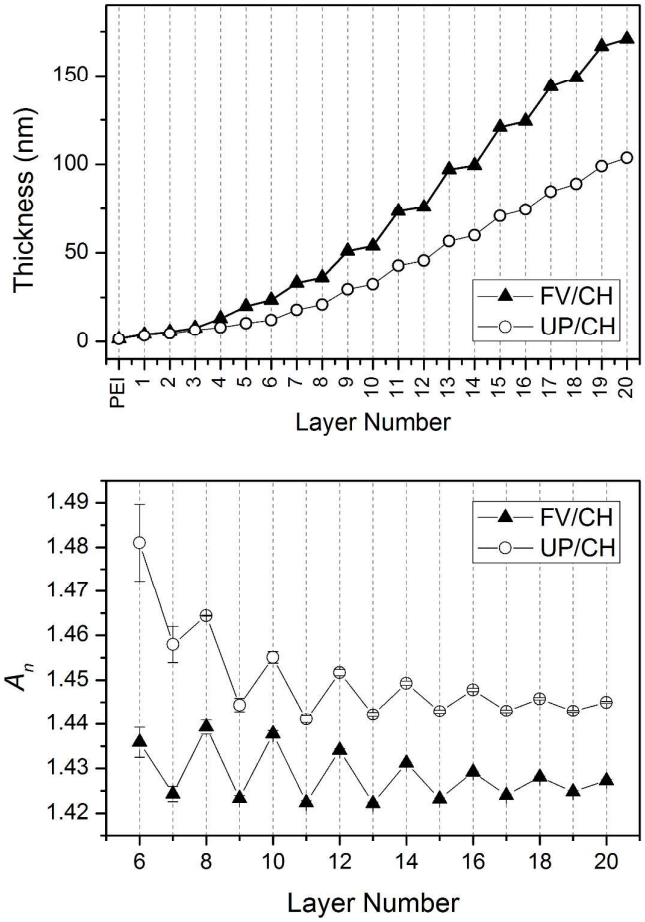

Figure 2: Ellipsometry data for the formation of fucoidan/chitosan multilayers on silicon wafers (from 500 ppm polymer solutions, 0.1 M KCl, pH 6) using both FV and UP. Thickness (top panel) and refractive index A_n parameter (bottom panel) of $(FV/CH)_{10}$ (black triangles) and $(UP/CH)_{10}$ (open circles) during build-up. Error in thickness values is < 0.5 nm for all datapoints. Error bars are included for A_n.

QCM-D

Frequency and dissipation changes of the QCM sensor were followed for multilayer build-up, with multiple overtones (3^{rd}, 5^{th}, 7^{th}, and 9^{th}) recorded for both $(FV/CH)_{10}$ and $(UP/CH)_{10}$ formation. Only the data for the 7^{th} overtone is presented in Figure 3 (full set of overtones is given in the supporting information). Figure 3 (top) shows the normalized frequency response as a function of time for both $(FV/CH)_{10}$ (black trace) and $(UP/CH)_{10}$ (grey trace), at each stage of the multilayer build-up. The first step in each trace represents: the addition of the PEI primer layer (15 min), followed by a KCl rinsing step (5 min); the subsequent addition of fucoidan (15 min), followed by a rinsing step (5 min); the subsequent addition of chitosan (15 min), followed by a rinsing step (5 min). The cycling of fucoidan and chitosan continued until the full 10-bilayer multilayer assembly was formed for both fucoidan systems. The final measured dissipation and frequency change for both multilayer systems produces values of between 1.2-1.3 x 10^{-8} Hz^{-1} for ratio of $\Delta D/(-\Delta f_n/n)$. This value allows us to assume that frequency change is proportional to mass gain for the entire build-up of both multilayers [50].

For both $(FV/CH)_{10}$ and $(UP/CH)_{10}$ the same general trend is observed in terms of frequency response for each stage of the adsorption. After an initial phase during which the first few layers attach to the surface (a process that is non-ideal for most multilayer systems), the build-up proceeds in a consistent step-wise fashion. The addition of fucoidan can be seen to cause a significant increase in the frequency change, followed by a small decrease during rinsing. This is due to adsorption of polymer, followed by removal of some loosely bound polymer during rinsing. The same pattern is observed for every fucoidan addition, for both FV and UP.

Addition of chitosan in the early stages is seen to follow a near identical pattern (significant frequency change, minor desorption upon rinsing). However, after the addition of the 4^{th}-5^{th} chitosan layer, the frequency change for each subsequent chitosan layer is small – indicating that the adsorption of chitosan does not result in a large gain of mass. In the case of UP/CH multilayer formation, the mass gain remains small but positive during the remaining build-up. However, for

FV/CH multilayer formation, the addition of chitosan eventually leads to an overall mass loss during build-up. The ellipsometry data (and zeta potential data) indicate that chitosan is adsorbing (and adsorbing in significant amounts), but the QCM data shows a reverse mass trend for FV/CH, presumably due to the significant displacement of hydration water during chitosan adsorption/interpenetration (QCM senses both solid polymer mass *plus* any associated hydration water). This is entirely consistent with the ellipsometry refractive index data shown in Figure 2. The same process will be happening during chitosan adsorption into the UP/CH multilayer, but the effect is more pronounced with the FV/CH multilayer.

The accompanying variation in the energy dissipation of the QCM sensor during multilayer build-up is given in Figure 3 (bottom) (also the 7^{th} overtone – full set of overtones is given in the supporting information). The initial settling-in period of the multilayer build-up (the first few bilayers) is more apparent in the dissipation data than the frequency data, and as with the frequency data, it settles into a consistent pattern after the 3^{rd} bilayer is reached. Although the trend is toward increasing dissipation with bilayer number, the actual behavior with addition of each individual polymer shows a saw-tooth pattern, with the dissipation increasing substantially with fucoidan addition, then decreasing upon addition of chitosan. This is seen for both multilayer systems, but is starker with the $(FV/CH)_{10}$ multilayer (in agreement with the expected larger changes in hydration water accompanying the cycling of fucoidan and chitosan, based on the frequency data). In addition, the UP fucoidan produces a less dissipative multilayer than the FV fucoidan, which is consistent with the previously presented ellipsometry data and parameters.

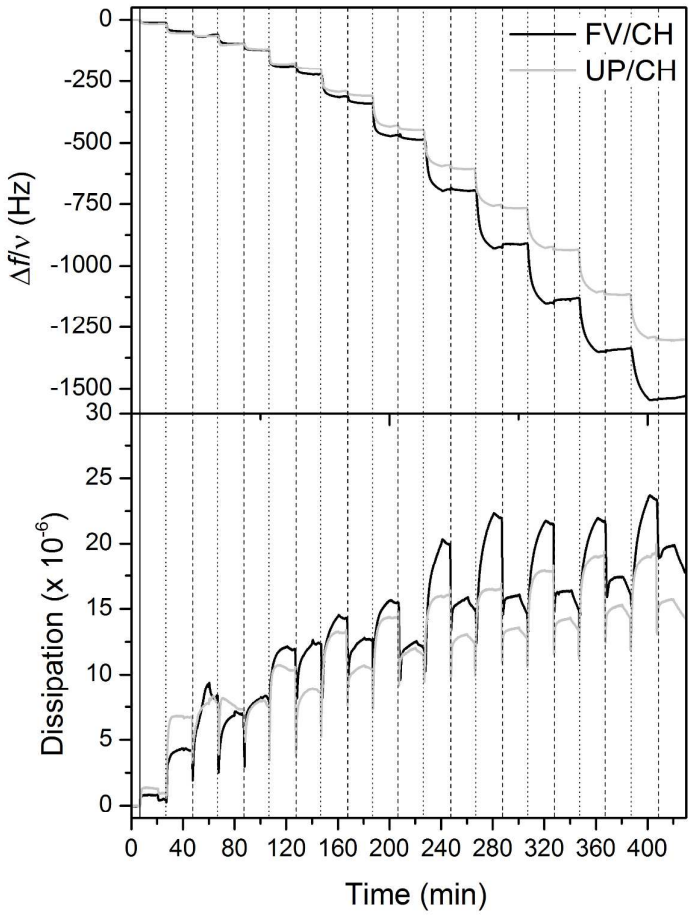

Figure 3: QCM-D plots for the formation of fucoidan/chitosan multilayers on silica-coated QCM sensors (from 500 ppm polymer solutions, 0.1 M KCl, pH 6) using both FV and UP. Normalized frequency (top panel) and dissipation change (bottom panel) for the 7th overtone for both $(FV/CH)_{10}$ (black traces) and $(UP/CH)_{10}$ (grey traces) multilayer systems. The solid vertical black line indicates the start of PEI adsorption. The vertical dotted lines indicate the start of fucoidan adsorption steps; the vertical dashed lines indicate the start of chitosan adsorption steps. There is a 5 min rinse stage before each addition of polymer.

Extra information can be obtained from the QCM data by plotting frequency directly against dissipation. *D-f* plots allow one to interrogate the rigidity/softness of adsorbed layers per unit 'mass' gain, and infer information on conformational change within the adsorbed layer [54-56]. They can also be used to get qualitative indications of such effects occurring during bilayer formation for polyelectrolyte multilayers [57]. *D-f* plots for 2 of the bilayer formation stages are shown in Figure 4 (the 5th and 9th bilayers for each system). For each bilayer, the dissipation and frequency at commencement of adsorption is set to zero to allow comparisons between two datasets for each multilayer. The top panel of Figure 4 contains the data for $(FV/CH)_{10}$. The data displayed for each bilayer includes the full fucoidan adsorption (stage 1 indicated on the plot): salt rinse (stage 2): chitosan adsorption (stage 3): and last salt rinse cycle (stage 4). Looking at the black symbol data for the 5th bilayer formation for $(FV/CH)_{10}$, it can be seen that the first sweep of the data is roughly linear during the fucoidan adsorption, with a slight upward trend from around 2/3 of the way through the adsorption, indicating a slightly looser conformation in the latter stages of adsorption. The rinse does little to alter the plot (small decrease in both frequency and dissipation, reflecting a small mass loss), but the addition of chitosan causes a significant downward sweep, followed by a linearly increasing region that ends with a slight dip due to rinsing. Exposure to the chitosan solution causes a significant change to the dissipation of the layer (which was also apparent in Figure 4), and most likely a significant conformational re-arrangement. The same trend is also observed for the 9th bilayer, although there is a lower slope for the fucoidan adsorption, i.e. a smaller change in dissipation per unit 'mass' gain for the fucoidan adsorption. The reduction in overall QCM-sensed mass during the later bilayer chitosan adsorption is seen in the *D-f* plot as a reverse in the frequency change direction in Figure 4 (step 3 – indicated in grey).

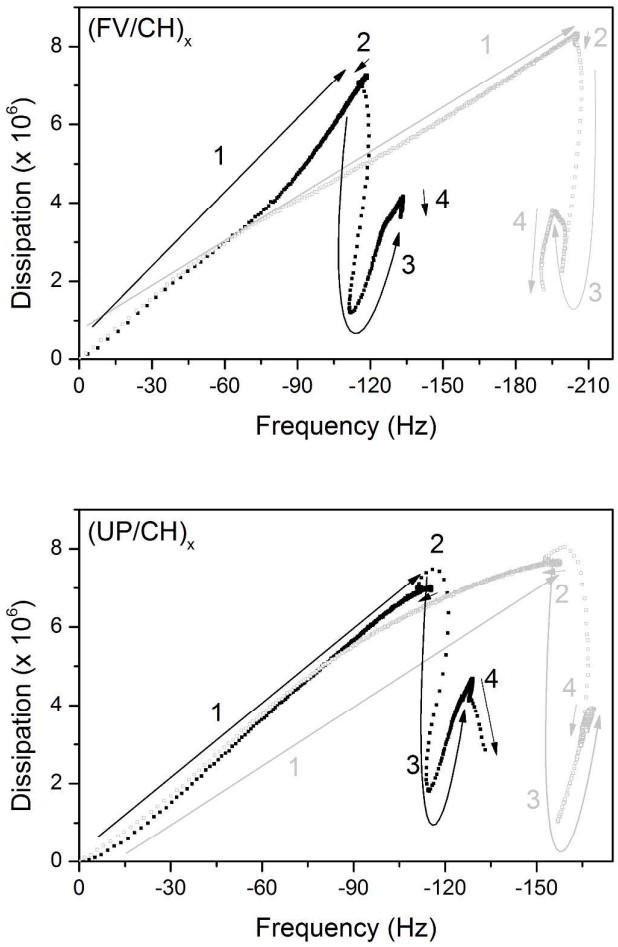

Figure 4: *D-f* plots for the formation of fucoidan/chitosan multilayers sensors (from 500 ppm polymer solutions, 0.1 M KCl, pH 6) using both FV and UP. Top – *D-f* plots (zeroed at the start of the adsorption stage) for $(FV/CH)_x$ for the 5th (black trace) and 9th (grey trace) bilayer formation. Bottom – *D-f* plots for $(UP/CH)_x$ for the 5th (black trace) and 9th (grey trace) bilayer formation. Stages of adsorption are indicated by numbers 1-4 (black for 5th bilayer; grey for 9th bilayer), as described in the text.

The lower panel in Figure 4 contains the data for $(UP/CH)_{10}$. There is a clear difference in this data compared to that for $(FV/CH)_{10}$. The slope of the D-f plot for the adsorption of fucoidan in each bilayer stage is non-linear but in the opposite direction (lower slope later in the fucoidan adsorption stage). For simple polymer adsorption onto a planar substrate, this is normally interpreted in terms of the individual adsorbed layer becoming more collapsed/dense as adsorption

proceeds to equilibrium. This explanation could hold for this case also, with UP fucoidan forming a denser conformation than FV when it adsorbs on top of a chitosan top layer. The changes in the data during chitosan adsorption are similar to that seen for FV, although there is no evidence of mass loss during chitosan adsorption, for either the 5th bilayer formation or 9th bilayer formation (step 3).

In addition to inspecting the frequency and dissipation response of the multilayer build-up, Voigt analysis was performed to enable calculation of the thickness and viscoelastic properties of the full 10-bilayer multilayers to be determined (film thickness d_{QCM}, the shear viscosity η_f, and the elastic modulus μ_f). The Qtools software (Q-sense, Sweden) was used to model the experimental data to obtain these parameters of the film. The changes in frequency in the 7th overtone and dissipation for the 7th and 9th overtones were fitted. The fixed values used in the model were: 0.001 kg/ms for background electrolyte viscosity, and 1000 kg/m^3 for the background electrolyte density. The value for the film density was chosen within a range between 1050 to 1400 kg/m^3 that provided the lowest χ^2 in the calculations, which in this case was 1150 kg/m^3.

Plots of the fitted frequency and dissipation data for both multilayer samples are given in the supporting information. The determined parameters for the multilayer assemblies with 10 bilayers are given in Table 3. The QCM-D Voigt analysis confirms that $(FV/CH)_{10}$ has a greater thickness (correlating well with the ellipsometry). The FV/CH multilayer can be seen to have a higher shear viscosity than the UP/CH multilayer, which is to be expected given the larger measured dissipation change for the formation of the FV/CH multilayer. The determined elastic modulus only varies by approx. 5% between the two multilayers, indicating only a small correlation between the structure/hydration content of the multilayers and the elastic response of the two multilayers. The calculation of these parameters is based on a number of assumptions concerning the composition, structure, and mechanical characteristics of the adsorbed multilayers. Therefore, some degree of caution is recommended when interpreting the determined values.

Table 3 – Parameters for $(FV/CH)_{10}$ and $(UP/CH)_{10}$, determined from QCM-D Voigt analysis (film thickness, d_{QCM}; shear viscosity, η_f; and the elastic modulus, μ_f)

	$(FV/CH)_{10}$	$(UP/CH)_{10}$
d_{QCM} (nm)	240.9	204.5
η_f (kg ms^{-1})	0.27	0.22
μ_f (x 10^6 Pa)	11.6	10.8

AFM Imaging

Adsorbed film morphology and thickness has been determined through the use of AFM imaging of the PEM films in the formation solvent (i.e. wet thickness). The use of intermittent contact imaging methodologies is essential when attempting to image adsorbed polymer layers [58]. Multilayer samples of 2, 4, 6, 8, and 10 bilayers were prepared on silicon wafer pieces by dip coating/rinsing. AFM images of the 10 bilayer samples of both $(FV/CH)_{10}$ and $(UP/CH)_{10}$ are given in Figure 5 (AFM images for samples of 2, 4, 6, and 8 bilayers are given in the supporting information). As detailed in the methodology section (and supporting information), each sample was scraped with a scalpel blade to reveal an area of underlying silicon wafer substrate. This allows the AFM image to reveal not just the morphology of the PEMs, but also their absolute thickness.

A detailed picture of the morphology of the multilayers during build-up can be seen by comparing the AFM images for the different samples with different multiples of bilayers (see supplementary information). In both cases, the layers consist of a film that completely covers the substrate, but is characterized by isolated island like features lying on top of the base film. Upon increasing the number of bilayers in the samples, the overall film thickness rises, and the island features grow larger and merge into larger features. By the time that 10-bilayers have been created, the films are over 380 nm thick and 239 nm thick, for $(FV/CH)_{10}$ and $(UP/CH)_{10}$, respectively (see Figure 5).

The image analysis allows one to look for differences between the two fucoidan polymers. A plot of thickness versus bilayer number is given in Figure 6. The (FV/CH) system can be seen to display the classic supra-linear/exponential growth in thickness, whereas the (UP/CH) displays a far

more linear increase in thickness with bilayer number (both observations are in agreement with the ellipsometry data presented in Figure 3). However, it needs to be highlighted here that the AFM data, the only direct measurement of multilayer height presented (ellipsometry and QCM thickness calculations are very model-dependent), give consistently higher thickness values than the data presented in Figure 2 and Table 3. The manner in which the average height was calculated from the AFM images (see supporting information) rules out the influence of surface roughness and PTV distances (which might be thought to bias the determined height to higher values), and therefore the AFM heights can be considered as accurate. This should serve as a note of caution for the use of solely ellipsometry and QCM to determine thickness values for polyelectrolyte multilayers.

The images of the PEMs also allow differences to be seen for the two systems. The (FV/CH) has a smaller number of larger island/lump features, compared to (UP/CH) which has a more compact layer but a larger number of smaller islands/lumps. This is reflected in the determined roughness parameters of the multilayers (see supplementary information).

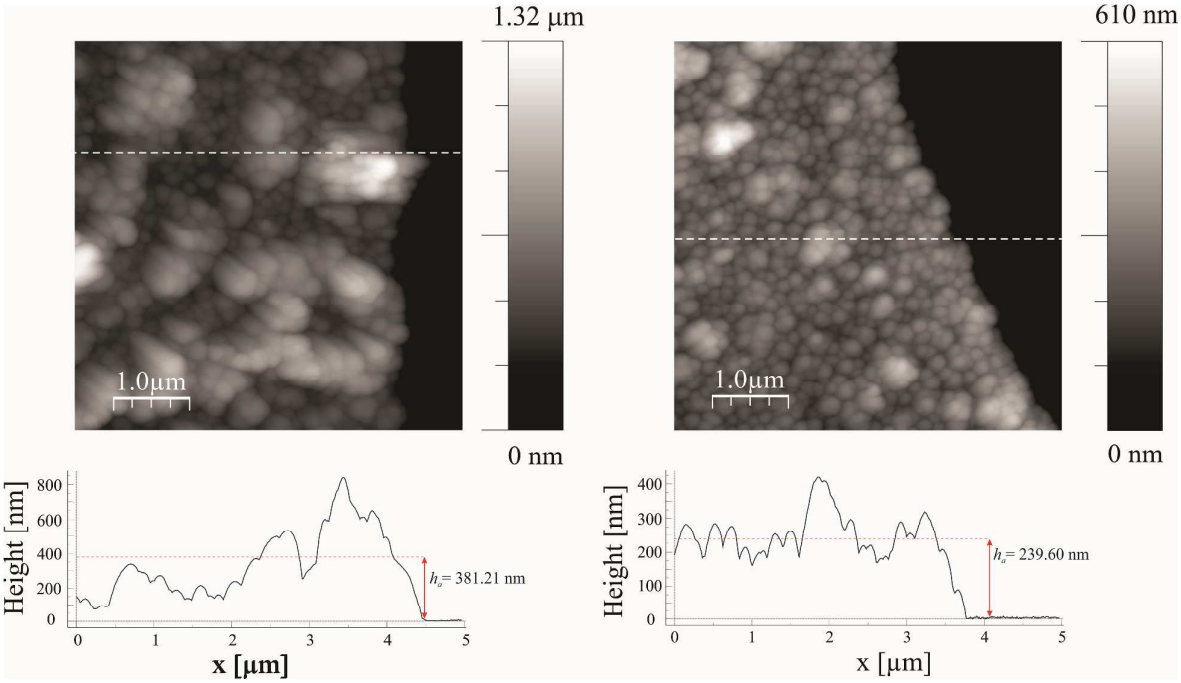

Figure 5: AFM 5 x 5 µm^2 height images of (A) $(FV/CH)_{10}$ and (B) $(UP/CH)_{10}$ multilayer samples, recorded in 0.1 M KCl, pH 6 electrolyte. Polymer solution concentrations for formation were 500 ppm. Below each AFM image is a 2D height cross section plot, which correlates with the dotted white line in each image.

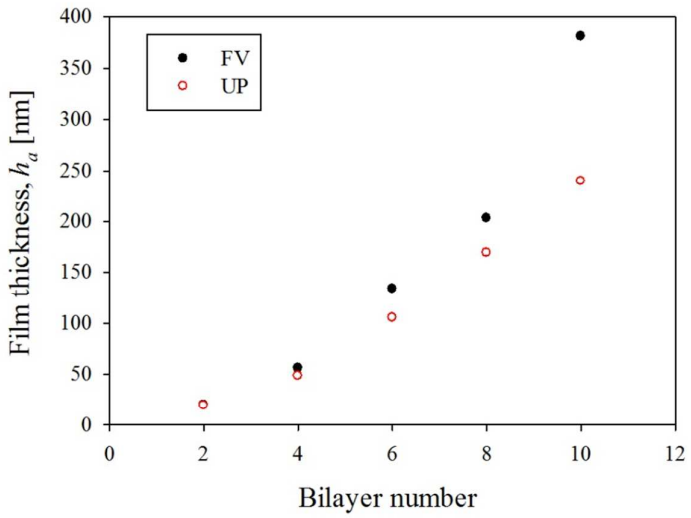

Figure 6: Plot of average height, h_a, versus bilayer number for 2, 4, 6, 8, and 10 bilayer samples of (FV/CH) and (UP/CH) multilayers. The average height is determined based on the height histograms of the AFM images presented in the supplementary information.

XPS

XPS has been used to interrogate the surface composition and chemistry of the fucoidan/chitosan multilayers. XPS is a very surface sensitive technique: for a polymer film on a solid support, an estimate can be made of the information depth from which the emitted photoelectrons will be sourced. Given the photon energy (1486.6 eV) and the binding energies of the photoelectrons emitted (between 160 eV and 400 eV), the emitted electron kinetic energies will yield an inelastic mean free path (IMFP) of approximately 3 nm for many organic materials, based on the equations of Tanuma, Powell, and Penn [59], and calculated by the QUASES-IMFP-TPP2M program [60]. This IMFP yields an information depth (ID_{90}) of approximately 7 nm (depth from which 90% of the signal is detected), based on the simple expression for ID without inclusion of elastic scattering interactions [61], and with the detector normal to the analysed surface (as was the case in this analysis). Given the layer thickness data in Figure 2, the XPS signal from the PEMs will be dominated by the last deposited layer (although drying the sample prior to measurement will go some way to reducing this dominance), therefore analysis has been performed on multilayers with varying final outer polymer layer: either chitosan terminated (which is an integer number of bilayers); or fucoidan terminated (which is a non-integer number of bilayers).

The surface atomic concentrations of 9.5- and 10-bilayer samples for both (FV/CH) and (UP/CH) multilayers is listed in Table 4, based on survey scans for each bilayer sample. The surface composition of the multilayers is dominated by carbon and oxygen, with smaller amounts of sulfur and nitrogen. This is consistent with the chemistry of the two polysaccharide polymers. The comparison between FV and UP for all samples reveals that the surface atomic concentrations are near identical irrespective of the fucoidan type. However, there is a distinct difference when one compares the 9.5- and 10-bilayer samples within one fucoidan type. For the 9.5-bilayer sample (with either FV or UP as the outer layer), there is a higher S concentration and a lower N concentration than for the 10-bilayer sample (with chitosan as the outer layer). This observation indicates that the depth from which photoelectrons are detected preferentially samples the topmost

layer of the multilayer. Also of interest is the detection of potassium counter-ions for the 9.5-bilayer samples. This signal is not from dried electrolyte solution, as there is no potassium observed with the chitosan polymer as the outer layer. These potassium atoms are most likely directly associated with the fucoidan sulfonate groups.

Table 4: Surface atomic concentrations, determined from XPS survey scans, for $(FV/CH)_{10}$, $(UP/CH)_{10}$, $(FV/CH)_{9.5}$, $(UP/CH)_{9.5}$.

Elements	$(FV/CH)_{9.5}$	$(FV/CH)_{10}$	$(UP/CH)_{9.5}$	$(UP/CH)_{10}$
O	41.7	39.8	41.2	39.2
C	50.2	52.8	50.7	53.2
N	3.2	4.2	3.7	4.6
S	4.3	3.2	4.1	3.0
K	0.6	-	0.3	-

More detail can be obtained on the chemistry of the multilayers from high resolution scans of the individual photoemission peaks. High resolution XPS spectra of the C 1*s*, N 1*s*, and S 2*p* photoelectron peaks of $(FV/CH)_x$ and $(UP/CH)_x$ PEMs are given in Figure 7 and Figure 8, respectively. Peak components for all elements for both FV and UP 9.5- and 10-bilayer samples, determined via peak fitting using CasaXPS, are given in Table 5. Additional XPS spectra for the bulk polymers (high res S 2*p*, O 1*s*, and C 1*s* spectra for bulk FV and UP; high res N 1*s*, C 1*s*, and O 1*s* for bulk chitosan) are provided in the supporting information.

Considering first the two sets of XPS spectra for FV/CH multilayers (top panels in Figure 7), the C 1*s* spectra reveal the presence of at least three different chemical environments. The deconvolution and fitting of C 1s spectral envelopes for polysaccharide PEMs is well-established [13, 27, 62]. A multilayer containing chitosan and FV fucoidan should have four chemical environments: (i) C-H; (ii) C-OH, C-O, and C-N; (ii) O-C-O; and (iv) N-C=O. The latter of these environments for the FV/CH multilayers only comes from the partially de-acetylated chitosan. All four environments are observed for the bulk chitosan polymer (see supporting information), and for the bulk FV fucoidan (with the fourth environment signal from O-C=O, rather than N-C=O, arising

presumably from uronic acid content of the bulk polymer sample). However, the peak deconvolution of the multilayer spectra cannot be fitted with four components without restricting either the peak widths or peak positions of the higher binding energy O-C-O and N-C=O components. The mixed nature of the systems (two different polysaccharides) has smeared the high binding energy tail of the C 1*s* envelope. The deconvolution shown in Figure 7 has three components (see Table 5), with a broader single component that most likely contains contributions from both O-C-O and N-C=O environments (the peak width is approx. 2 eV, which is broader than the expected natural linewidths and spectral resolution of the XPS instrument). Also of note in the C 1*s* spectra is the observation of the K 2*p* doublet in the $(FV/CH)_{9.5}$ multilayer, reflecting the association of the cation counter-ion to the anionic sulfonate group within the multilayer when fucoidan is the exposed top surface of the multilayer: not all sulfonate groups are interacting with chitosan ammonium groups.

The S 2*p* spectra for the 9.5- and 10-bilayer FV/CH multilayers are shown in the central two panels of Figure 7. For both multilayers, the position of the sulfur photoemission peak envelope is representative of sulfoxy (SO) species, and is commonly observed at this position in the XPS spectra of PEMs containing sulfated polysaccharides like heparin and carrageenan [63, 64], in addition to single adsorbed layers of fucoidan [65]. The S 2*p* photoemission peak for a single sulfur chemical environment is a spin orbit doublet: $2p_{3/2}$ and $2p_{1/2}$. These two components need to be fitted with identical peak widths, a peak ratio of 2:1, and a fixed peak position of difference of 1.19 eV. These quantum mechanical constraints allow for the fitting of complex S 2*p* envelopes without any need to arbitrarily constrain peak widths or positions [66]. In the two examples in Figure 7, a single peak doublet with these specific fitting constraints cannot fit either the $(FV/CH)_{9.5}$ or $(FV/CH)_{10}$ S 2*p* peak envelope. Two doublets are required. The need for two doublets is most apparent for the $(FV/CH)_{9.5}$ multilayer.

The FV fucoidan should only have one distinct chemical environment for the sulfonate group, based on the chemical structure in Figure 1. However, the two peak doublets indicate that the

interactions of the fucoidan sulfonate group with the other components of the multilayer (cations/polycations) have altered the environment of at least some of the sulfonates. It should be noted that the S 2*p* region for the bulk FV polymer also has two doublets (see supporting information), presumably due to association with cations present in the material. Similar multiple doublets have been observed for the sulfonate S 2*p* region of XPS spectra of precipitates of poly styrene sulfonate (PSS) with poly 4-vinyl pyridine (P4VP) [67]; in this case, the appearance of a second, lower energy doublet, is interpreted as being due to the removal of the zinc counterion from the PSS during the formation of the precipitates. Based on our observations and the above-mentioned literature data, we assign the higher binding energy doublet of fucoidan to the charged sulfonate group in a direct cation/polycation ion-pair interaction.

It can be seen that the interacting peak doublet (higher binding energy) is dominant in the $(FV/CH)_{9.5}$ multilayer spectrum (see Table 5), indicating that the majority of the sulfonate groups are directly ion-paired, either with a potassium counter ion, or with chitosan ammonium groups, when the fucoidan polymer is exposed at the top surface of the multilayer. The situation is reversed when the chitosan layer terminates the multilayer. It is possible that, as with PSS association with P4VP (in which a zinc counterion is displaced), the interaction with chitosan displaces the potassium counterion from the fucoidan (see C 1*s* spectra in Figure 7), but does not always replace it with a direct ammonium ion-pair interaction.

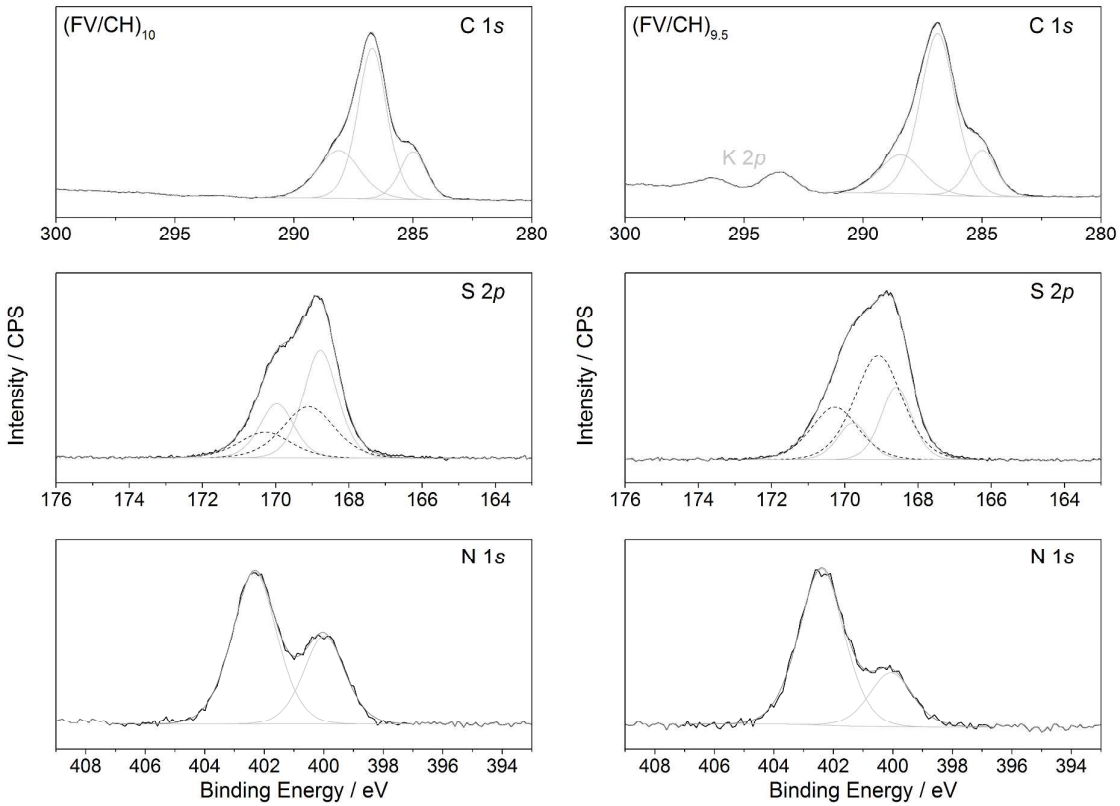

Figure 7: XPS High Resolution Spectra: LEFT - $(FV/CH)_{10}$ and RIGHT – $(FV/CH)_{9.5}$). Top – C 1*s* spectra; middle – S 2*p* spectra; bottom – N 1*s* spectra. Spectra fitted using CasaXPS. Multilayers formed on silicon wafer substrates from 500 ppm polymer solutions, 0.1 M KCl, pH 6. Dotted lines in the peak deconvolution of the S 2*p* envelope indicate a second peak doublet.

The lower two panels in Figure 7 have the N 1*s* spectra for $(FV/CH)_{10}$ and $(FV/CH)_{9.5}$. The N 1*s* peak profile consists of two components representing different chemical environments for the chitosan nitrogens. This functional group of the chitosan can be neutral ($-NH_2$ amine) or positively charged ($-NH_3^+$ ammonium). The component at approx. 400 eV is the neutral amine peak; the component at approx. 402 eV is the charged ammonium peak [27, 65, 68]. The lower binding energy peak also has a contribution from amide from acetylated chitosan sections, although the peak profile does not require the addition of a third peak component, as is sometimes the case with chitosan multilayers with heparin [13, 27]. As the spectra did not have a clear indication of a third peak component with a significantly different peak position within the peak envelope, the fit was completed with just the two peak components. It should be noted that spectra reported by other authors for synthetic polymers adsorbed from solution, with the polymer containing all three nitrogen environments, were also fitted in this manner [68], with a single peak component to account for both uncharged nitrogen environments (amine and amide).

It is the lower binding energy component ($-NH_2$ and –NH-C=O) that dominates the N 1*s* spectrum of bulk chitosan powder, in agreement with previously published spectra of bulk chitosan [69, 70]. The formation of a protonated, hydrated film of chitosan at the pH used in this study for PEM formation (pH 6) results in significant increase in the peak due to charged ammonium; as mentioned in the materials section, the pKa of chitosan is approx. 6.5 [40], indicating that at pH 6, a significant amount of the chitosan monomers will have ammonium rather than amide groups.

Of particular note in the XPS spectra of the N 1*s* region for the $(FV/CH)_{10}$ and $(FV/CH)_{9.5}$ multilayers in Figure 7 is a variation in the ratio of the two peak components. The overall percentage of N detected at the surface of the $(FV/CH)_{10}$ multilayer is higher (see Table 4) than for the $(FV/CH)_{9.5}$ multilayer, as expected due to chitosan being the terminating polymer layer in the $(FV/CH)_{10}$ multilayer (and thus more readily detected with XPS). In addition, the high resolution spectra indicate that there is a relative increase in the amount of $–NH_2$ compared to $–NH_3^+$ detected when chitosan is the terminating layer. There are two potential explanations for this latter

observation. The first explanation is that the local pH within the multilayer is slightly lower than the bulk solution, which could result in a greater degree of protonation of the chitosan within the multilayer, compared to a terminating chitosan layer, which will be more influenced by the bulk solution pH. Local pH in PEMs is known to be a factor in the swelling of PEM systems in response to bulk solution pH change [71], and can also be influenced directly using electrochemical methods [72]. The second possibility is that sample drying has had a differential effect on the chitosan within the PEM relative to the chitosan at the surface of the PEM, i.e. ion paired ammonium groups within the layer may retain their ionic character during drying, whereas 'free' ammonium groups at the surface of the PEM may protonate during drying more readily. We cannot be sure which of these two reasons is most likely from the data obtained, as XPS is an *ex situ* technique. Nevertheless, the XPS spectra indicate that there is some difference in the N environment for chitosan at the very top surface of the multilayer relative to that inside the layer.

The accompanying XPS spectra of the two UP fucoidan/chitosan multilayers are given in Figure 8. In general, the spectra of the three element regions are remarkably similar to those for the FV multilayers (as expected to some degree, given the similarity of the bulk polymer chemistry – and the bulk polymer XPS spectra – see supporting information). The same assignments can be made for all spectra, and the same general trends can be seen when comparing the 9.5-bilayer spectra with those of the 10-bilayer spectra (complete multilayer has lower cation/polycation interacting S 2*p*; complete multilayer has increased N at the surface, and an increased amount of the lower binding energy component in the high res N 1*s* spectrum). The differences between the two fucoidans only become apparent when one inspects the actual percentage contributions of the peaks from the peak fitting process (see Table 4). Irrespective of the outer layer probed, the UP multilayers have a lower proportion of interacting sulfonate (cation/polycation) and a larger percentage of the lower binding energy non-charged amine N 1*s* peak component than the FV multilayers. The XPS data indicates that ion-pairing between chitosan and fucoidan is reduced for UP relative to FV.

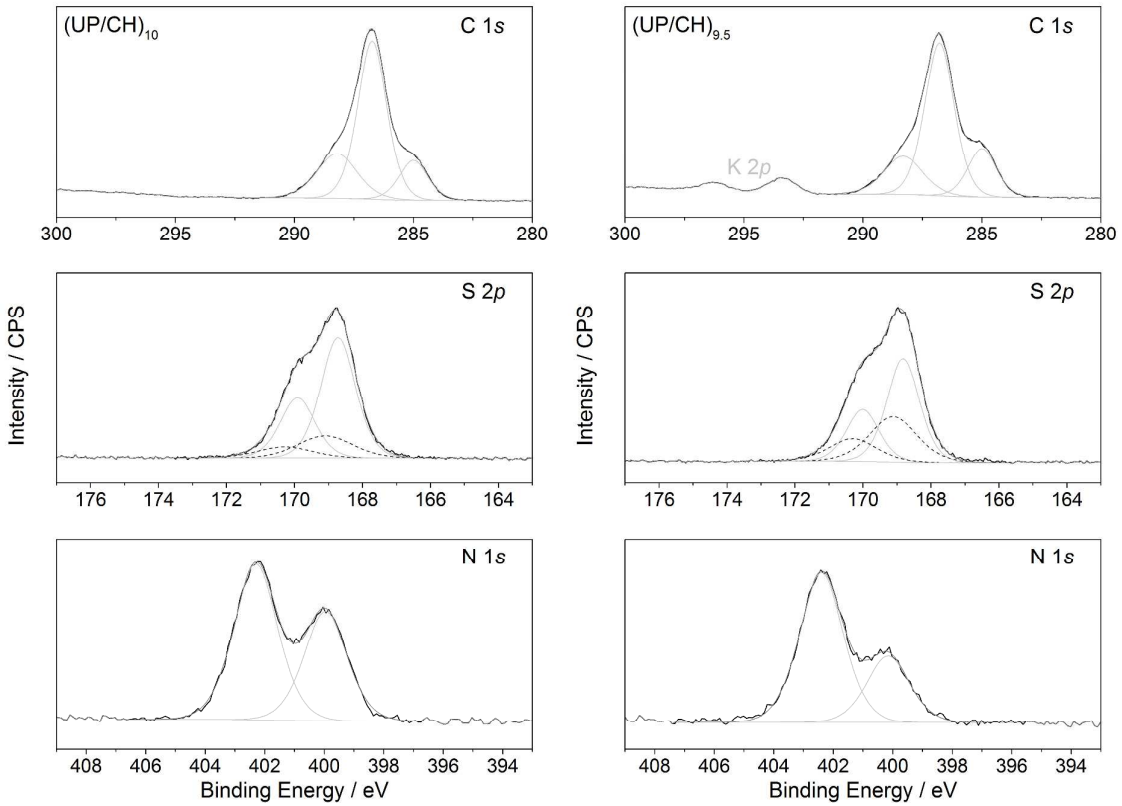

Figure 8: XPS High Resolution Spectra: LEFT - $(UP/CH)_{10}$ and RIGHT – $(UP/CH)_{9.5}$). Top – C 1*s* spectra; middle – S 2*p* spectra; bottom – N 1*s* spectra. Spectra fitted using CasaXPS. Multilayers formed on silicon wafer substrates from 500 ppm polymer solutions, 0.1 M KCl, pH 6. Dotted lines in the peak deconvolution of the S 2*p* envelope indicate a second peak doublet.

Table 5: XPS peak positions, relative abundance, and peak widths for the components of the C 1*s*, S 2*p*, and N 1*s* spectra from $(FV/CH)_{10}$, $(FV/CH)_{9.5}$, $(UP/CH)_{10}$, and $(UP/CH)_{9.5}$ multilayers. Only the peak position of the S $2p_{3/2}$ component is given in the table for the two different S chemical environments (the S $2p_{1/2}$ component is 1.19 eV higher in energy).

Element	Binding Energy	Abundance (%)	FWHM (eV)	Binding Energy	Abundance (%)	FWHM (eV)	Assignment [a]
		$(FV/CH)_{10}$			$(FV/CH)_{9.5}$		
C 1*s*	285.0	17	1.3	285.0	15	1.4	C-H
	286.7	57	1.4	286.9	66	1.7	C-OH, C-N, C-O
	288.1	26	2.0	288.0	19	2.1	O-C-O/C=O, N-C=O
S $2p_{3/2}$	168.8	58	1.1	168.6	31	1.0	SO_3^-
	169.1	42	1.6	169.6	69	1.5	interacting SO_3^-
N 1*s*	400.0	35	1.6	400.1	25	1.7	$-NH_2$, -NH-C=O
	402.3	65	1.7	402.4	75	2.4	$-NH_3^+$
		$(UP/CH)_{10}$			$(UP/CH)_{9.5}$		
C 1*s*	285.0	15	1.4	285.0	19	1.4	C-H
	286.7	61	1.4	286.8	61	1.4	C-OH, C-N, C-O
	288.2	24	2.0	288.0	20	1.9	O-C-O/C=O, N-C=O
S $2p_{3/2}$	168.7	78	1.2	168.8	61	1.1	SO_3^-
	169.1	22	1.9	169.1	39	1.6	interacting SO_3^-
N 1*s*	400.0	41	1.7	400.1	30	1.3	$-NH_2$, -NH-C=O
	402.3	59	1.7	402.4	70	2.4	$-NH_3^+$

[a] for references, see main text.

DISCUSSION

The data presented above provide a detailed picture of the formation and characteristics of the two multilayer samples. The two fucoidan polymers differ in a number of important respects that allow us to interpret and explain the majority of the observations. FV has a more consistent monomer composition, and thus a uniform substitution point for the sulfonate group. It also has a higher peak molecular weight than UP. UP has a more diverse monomer composition, a significant structural variation in the substitution point of the sulfonate, and the presence of acetyl groups as additional functionality. However, both polymers have a similar percentage of sulfonation.

The XPS and zeta potential data (see S1 for zeta potential data) for the two multilayer systems in some respects reflect the overall similarity of the two fucoidan polymers, rather than their differences. The XPS data indicates that there is a similar compositional make-up of the multilayers, even for multilayers with different terminating polymers. The zeta potential data indicate that both fucoidans produce the expected saw-tooth variation in charge with cycling of polyanion and polycation. The XPS data reveal subtle differences in ion-pairing between the two fucoidans when UP is compared to FV (less ion-pairing in UP multilayers), and the zeta potential data indicate that there are slight differences in the extent of positive potential relative to negative potential for FV and UP.

The differences detected in the zeta potential and XPS data are amplified in the data for the two systems from the AFM imaging, ellipsometry, and QCM-D. In all of these experiments, the larger peak molecular weight of FV relative to UP could be used to explain the differences. A higher molecular weight polymer would be expected to result in an adsorbed fucoidan layer that has a greater thickness, and a conformation that would allow easier migration and inter-digitation of chitosan into the adsorbed fucoidan layers during polycation adsorption. In contrast, UP would appear to reduce the interpenetration of chitosan into the multilayer structure during build-up, although some interpenetration does still occur, as evidenced by the QCM-D data (frequency and dissipation change values shown in Figure 3) and the ellipsometry refractive index values (Figure

2). However, caution should be exercised here, as both polymers are polydisperse, and as mentioned in the materials section, UP does have a significant proportion of polymer chains with very high molecular weights. It is possible that molecular weight differences are a contributing factor to the differences in the multilayer properties, but it is likely that there are other contributing factors.

The effect of varied polymer chemistry between the two fucoidans is one such factor. UP has two specific structural/chemical differences that could account for an altered interaction with chitosan relative to the interaction between FV and chitosan: sugar monomer differences and presence of acetylation. UP has sulfonation from two different sugar monomers (see Figure 1), which may present a higher degree of conformational flexibility in ensuring good ion-pairing between the amine groups on chitosan and the sulfonate groups on the fucoidan. Increased ion-pairing would be expected to reduce the hydration of the polymer film (reducing the hydration water surrounding charged groups). However, the XPS data indicate that UP has a lower degree of ion-pairing, so this structural variation cannot be used to explain the differences in structure and build-up between the two multilayer systems.

It is therefore most probable that the acetylation of UP is the major factor in altering the properties of the multilayer relative to the FV multilayer. First, as the acetyl group is a slightly hydrophobic moiety, its presence within the multilayer could contribute to the lower measured hydration of the UP/CH multilayer system. Second, acetyl groups provide an additional binding interaction between the two polymers. Both chitosan and UP fucoidan contain acetyl groups – which are known as potential sites for the formation of hydrogen bonding between chitin and chitosan chains [40]. The combination of acetyl groups on both polyanion and polycation will result in additional hydrogen bonding interactions between the polymers, resulting in a thinner, less hydrated layer. This interpretation aligns with the *D-f* plots shown in Figure 9; the addition of UP fucoidan results in a curved *D-f* plot region, with the direction of the curve (gradient decreasing as adsorption progresses) indicating a more collapsed/condensed conformation as the UP layer

adsorption reaches equilibrium. Choosing fucoidan and chitosan polymers with particular degrees of acetylation may be a simple strategy to produce multilayers of controlled properties.

Of additional interest from the datasets generated and reported here is how these fucoidan-based multilayers compare to those formed from chitosan with other sulfated polysaccharides (heparin, carrageenan, etc.) [18, 63, 64, 73, 74]. Carrageenans are of much higher molecular range to fucoidan, and thus present a good direct comparison in studies of PEM films formed with chitosan [63, 74]. Carrageenan/chitosan multilayers are seen to form relatively similar morphologies to fucoidan/chitosan, when investigated using AFM imaging [63, 74]. In addition, the layer thickness determined via optical techniques for the two systems is similar (i.e. in the 100s of nm range).

For comparisons with heparin, there are chemical differences (heparin contains both carboxyl and sulfonate anion groups), but also significant molecular weight differences. Heparin is a small polymer (around 15,000 Dalton), and multilayers formed with chitosan and heparin are much thinner when compared to the multilayers formed in this work [18, 64]. The relative size of chitosan to the anionic polysaccharide is also a major factor in the behaviour of the multilayers during formation. In the work presented here, chitosan is seen to migrate into the topmost fucoidan layer, resulting in densification upon addition of the polycation – as seen in the ellipsometry/refractive index data shown in Figure 6. For heparin/chitosan multilayers studied by Lundin et al. [18] (who study adsorption under similar pH and ionic strength to that used in the current study), similar 'saw-tooth' profiles are seen for refractive index when the multilayer is exposed to chitosan during formation (rise in refractive index, followed by a fall in value upon exposure to the polyanion). Also similar to the current work, is the rise in layer thickness with addition of the heparin polyanion in the work of Lundin et al., although given the small size of the heparin relative to the fucoidan, it is possible that the mechanism of film thickness increase is different. Heparin most likely acts to swell up the adsorbed chitosan layer, with polyanion and hydration water. In this work, fucoidan will act as a framework into which the chitosan can penetrate/migrate.

CONCLUSION

Fucoidan chemistry has been demonstrated to have a strong influence on polyelectrolyte multilayer properties. Multilayers of fucoidan/chitosan formed with fucoidan extracted from *Undaria pinnatifida* produce thinner, denser, smoother multilayers than the corresponding multilayer system using fucoidan extracted from *Fucus vesiculosus*. In addition to some influence of molecular weight variation between the two fucoidans, the presence of additional acetyl groups on the UP fucoidan is the most likely explanation for the observed differences. Acetyl groups provide a functionality that allows for additional interactions between the UP fucoidan and chitosan, through intermolecular hydrogen bonding, similar to that which occurs between chitin molecules or between partially acetylated chitosan molecules. Choosing fucoidan polymers (and chitosan) with specific degree of acetylation will allow for the production of tailored multilayers for applications requiring soft matter surface coatings.

ACKNOWLEDGEMENTS

The authors would like to think Professors Vincent Ball, Michal Borkovec, and Helmuth Möhwald, for their valuable comments and suggestions on the manuscript. This work was funded by the Australian Research Council through the Future Fellowship awarded to DB (FT100100393). TH acknowledges the financial support of Division of Health Sciences and the School of Pharmacy and Medical Sciences of UniSA for her scholarship support. This work was performed in part at the South Australian node of the Australian National Fabrication Facility, a company established under the National Collaborative Research Infrastructure Strategy to provide nano and micro-fabrication facilities for Australia's researchers.

Electronic Supplementary Information Available: XPS of bulk polymers; AFM images of 2, 4, 6, 8, and 10 bilayer multilayers; ellipsometry data; QCM data and Voigt fits. This material is available free of charge via the Internet at www.rsc.org/softmatter

REFERENCES

1. G. Decher, *Science*, 1997, **277**, 1232-1237.
2. J. B. Schlenoff, *Langmuir*, 2009, **25**, 14007-14010.
3. H. Kerdjoudj, N. Berthelemy, F. Boulmedais, J.-F. Stoltz, P. Menu and J. C. Voegel, *Soft Matter*, 2010, **6**, 3722-3734.
4. R. R. Costa and J. F. Mano, *Chemical Society Reviews*, 2014, **43**, 3453-3479.
5. E. Wischerhoff, N. Badi, J.-F. Lutz and A. Laschewsky, *Soft Matter*, 2010, **6**, 705-713.
6. J. L. Lutkenhaus and P. T. Hammond, *Soft Matter*, 2007, **3**, 804-816.
7. T. Crouzier, T. Boudou and C. Picart, *Curr. Opin. Colloid Interface Sci.*, 2010, **15**, 417-426.
8. B. B. Hsu, S. R. Hagerman, K. Jamieson, J. Veselinovic, N. O'Neill, E. Holler, J. Y. Ljubimova and P. T. Hammond, *Biomacromolecules*, 2014, **15**, 2049-2057.
9. J. H. H. Bongaerts, J. J. Cooper-White and J. R. Stokes, *Biomacromolecules*, 2009, **10**, 1287-1294.
10. D. A. Beattie, A. Beaussart, A. Mierczynska-Vasilev, S. L. Harmer, B. Thierry, L. Puskar and M. Tobin, *Langmuir*, 2012, **28**, 1683-1688.
11. B. Thierry, F. M. Winnik, Y. Merhi, J. Silver and M. Tabrizian, *Biomacromolecules*, 2003, **4**, 1564-1571.
12. B. Wu, G. Liu, G. Zhang and V. S. J. Craig, *Soft Matter*, 2014, **10**, 3806-3816.
13. J. Almodóvar, J. Mower, A. Banerjee, A. K. Sarkar, N. P. Ehrhart and M. J. Kipper, *Biotechnol. Bioeng.*, 2013, **110**, 609-618.
14. N. Saha, C. Monge, V. Dulong, C. Picart and K. Glinel, *Biomacromolecules*, 2013, **14**, 520-528.
15. F. J. Pavinatto, L. Caseli and O. N. Oliveira, *Biomacromolecules*, 2010, **11**, 1897-1908.
16. C. R. Correia, P. Sher, R. L. Reis and J. F. Mano, *Soft Matter*, 2013, **9**, 2125-2130.

17. F. Cuomo, F. Lopez, A. Ceglie, L. Maiuro, M. G. Miguel and B. Lindman, *Soft Matter*, 2012, **8**, 4415-4420.
18. M. Lundin, F. Solaqa, E. Thormann, L. Macakova and E. Blomberg, *Langmuir*, 2011, **27**, 7537-7548.
19. A. Guyomard, G. Muller and K. Glinel, *Macromol.*, 2005, **38**, 5737-5742.
20. T. Serizawa, M. Yamaguchi and M. Akashi, *Biomacromolecules*, 2002, **3**, 724-731.
21. L. Shen, P. Chaudouet, J. Ji and C. Picart, *Biomacromolecules*, 2011, **12**, 1322-1331.
22. J. F. Quinn, S. J. Pas, A. Quinn, H. P. Yap, R. Suzuki, F. Tuomisto, B. S. Shekibi, J. I. Mardel, A. J. Hill and F. Caruso, *Journal of the American Chemical Society*, 2012, **134**, 19808-19819.
23. J. Zhou, B. Wang, W. Tong, E. Maltseva, G. Zhang, R. Krastev, C. Gao, H. Möhwald and J. Shen, *Colloid Surf. B*, 2008, **62**, 250-257.
24. M. Westwood, T. R. Noel and R. Parker, *Biomacromolecules*, 2010, **12**, 359-369.
25. D. Volodkin and R. Von Klitzing, *Curr. Opin. Colloid Interface Sci.*, 2014, **19**, 25-31.
26. T. Crouzier and C. Picart, *Biomacromolecules*, 2009, **10**, 433-442.
27. J. Almodóvar, L. W. Place, J. Gogolski, K. Erickson and M. J. Kipper, *Biomacromolecules*, 2011, **12**, 2755-2765.
28. M. Z. Markarian, M. D. Mousallem, H. W. Jomaa and J. B. Schlenoff, *Biomacromolecules*, 2007, **8**, 59-64.
29. E. Kharlampieva and S. A. Sukhishvili, *Macromolecules*, 2003, **36**, 9950-9956.
30. N. A. Kotov, *Nanostructured Materials*, 1999, **12**, 789-796.
31. R. R. Costa, A. M. Testera, F. J. Arias, J. C. Rodríguez-Cabello and J. F. Mano, *Journal of Physical Chemistry B*, 2013, **117**, 6839-6848.
32. N. Aggarwal, N. Altgarde, S. Svedhem, K. Zhang, S. Fischer and T. Groth, *Colloid Surf. B*, 2014, **116**, 93-103.
33. H. D. M. Follmann, A. F. Martins, A. P. Gerola, T. A. L. Burgo, C. V. Nakamura, A. F. Rubira and E. C. Muniz, *Biomacromolecules*, 2012, **13**, 3711-3722.
34. M. I. Bilan, A. A. Grachev, N. E. Ustuzhanina, A. S. Shashkov, N. E. Nifantiev and A. I. Usov, *Carbohydrate Research*, 2002, **337**, 719-730.
35. A. O. Chizhov, A. Dell, H. R. Morris, S. M. Haslam, R. A. McDowell, A. S. Shashkov, N. E. Nifant'ev, E. A. Khatuntseva and A. I. Usov, *Carb. Res.*, 1999, **320**, 108-119.
36. P. X. Sheng, Y.-P. Ting, J. P. Chen and L. Hong, *Journal of Colloid and Interface Science*, 2004, **275**, 131-141.
37. J. H. Fitton, *Marine Drugs*, 2011, **9**, 1731-1760.
38. R. Cooper, C. Dragar, K. Elliot, J. H. Fitton, J. Godwin and K. Thompson, *BMC Complementary and Alternative Medicine*, 2002, **2**.
39. T. Indest, J. Laine, K. S. Kleinschek and L. F. Zemljič, *Colloid Surf. A*, 2010, **360**, 210-219.
40. C. K. S. Pillai, W. Paul and C. P. Sharma, *Prog. Poly. Sci.*, 2009, **34**, 641-678.
41. I. Szilagyi, G. Trefalt, A. Tiraferri, P. Maroni and M. Borkovec, *Soft Matter*, 2014, **10**, 2479-2502.
42. M. Ferriz-Mañas and J. B. Schlenoff, *Langmuir*, 2014, **30**, 8776-8783.
43. M. H. Rogers and G. N. Lance, *J. Fluid Mech.*, 1960, **7**, 617-631.
44. P. J. Sides, J. Newman, J. D. Hoggard and D. C. Prieve, *Langmuir*, 2006, **22**, 9765-9769.
45. I. Horcas, R. Fernandez, J. M. Gomez-Rodriguez, J. Colchero, J. Gomez-Herrero and A. M. Baro, *Rev. Sci. Instr.*, 2007, **78**, 013705.
46. M. Born and E. Wolf, *Principles of Optics: Electromagnetic Theory of Propagation, Interference and Diffraction of Light*, Cambridge University Press, Cambridge, 1999.
47. J. A. De Feijter, J. Benjamins and F. A. Veer, *Biopolymers*, 1978, **17**, 1759-1772.
48. F. Höök, M. Rodahl, P. Brzezinski and B. Kasemo, *Langmuir*, 1998, **14**, 729-734.
49. G. Sauerbrey, *Zeitschrift fur Physik A: Hadrons and Nuclei*, 1959, **155**, 206-222.
50. I. Reviakine, D. Johannsmann and R. P. Richter, *Analytical Chemistry*, 2011, **83**, 8838-8848.

51. M. V. Voinova, M. Rodahl, M. Jonson and B. Kasemo, *Physica Scripta*, 1999, **59**, 391.
52. D. A. Shirley, *Physical Review B: Condensed Matter*, 1972, **5**, 4709.
53. C. Picart, J. Mutterer, L. Richert, Y. Luo, G. D. Prestwich, P. Schaaf, J.-C. Voegel and P. Lavalle, *Proc. Nat. Acad. Sci.*, 2002, **99**, 12531-12535.
54. A. Monkawa, T. Ikoma, S. Yunoki, T. Yoshioka, J. Tanaka, D. Chakarov and B. Kasemo, *Biomaterials*, 2006, **27**, 5748-5754.
55. F. Hook, M. Rodahl, P. Brzezinski and B. Kasemo, *Langmuir*, 1998, **14**, 729-734.
56. I. G. Sedeva, D. Fornasiero, J. Ralston and D. A. Beattie, *Langmuir*, 2010, **26**, 15865-15874.
57. A. Barrantes, O. Santos, J. Sotres and T. Arnebrant, *Journal of Colloid and Interface Science*, 2012, **388**, 191-200.
58. M. Krasowska, A. Niecikowska and D. A. Beattie, *Surface Innovations*, 2014, **2**, 151-159.
59. S. Tanuma, C. J. Powell and D. R. Penn, *Surface and Interface Analysis*, 1994, **21**, 165-176.
60. S. Tougaard, 2010, QUASES-IMFP-TPP2M, http://www.quases.com/products/quases-imfp-tpp2m/
61. A. Jablonski and C. J. Powell, *Journal of Vacuum Science and Technology A: Vacuum, Surfaces and Films*, 2003, **21**, 274-283.
62. C. D. Easton, A. J. Bullock, G. Gigliobianco, S. L. McArthur and S. MacNeil, *Journal of Materials Chemistry B*, 2014, **2**, 5558-5568.
63. S. Bratskaya, D. Marinin, F. Simon, A. Synytska, S. Zschoche, H. J. Busscher, D. Jager and H. C. van der Mei, *Biomacromolecules*, 2007, **8**, 2960-2968.
64. S. Boddohi, C. E. Killingsworth and M. J. Kipper, *Biomacromolecules*, 2008, **9**, 2021-2028.
65. T. Indest, J. Laine, L.-S. Johansson, K. Stana-Kleinschek, S. Strnad, R. Dworczak and V. Ribitsch, *Biomacromolecules*, 2009, **10**, 630-637.
66. D. A. Beattie, I. M. Kempson, L.-J. Fan and W. M. Skinner, *Int. J. Miner. Process.*, 2009, **92**, 162-168.
67. S. H. Goh, S. Y. Lee, X. Zhou and K. L. Tan, *Macromol.*, 1998, **31**, 4260-4264.
68. O. J. Rojas, M. Ernstsson, R. D. Neuman and P. M. Claesson, *Journal of Physical Chemistry B*, 2000, **104**, 10032-10042.
69. G. Lawrie, I. Keen, B. Drew, A. Chandler-Temple, L. Rintoul, P. Fredericks and L. Grondahl, *Biomacromolecules*, 2007, **8**, 2533-2541.
70. L. Dambies, C. Guimon, S. Yiacoumi and E. Guibal, *Colloid Surf. A*, 2001, **177**, 203-214.
71. P. M. Biesheuvel, T. Mauser, G. B. Sukhorukov and H. Möhwald, *Macromolecules*, 2006, **39**, 8480-8486.
72. D. J. Schmidt, Y. Min and P. T. Hammond, *Soft Matter*, 2011, **7**, 6637-6647.
73. J. Fu, J. Ji, W. Yuan and J. Shen, *Biomaterials*, 2005, **26**, 6684-6692.
74. S. M. Oliveira, T. H. Silva, R. L. Reis and J. F. Mano, *Journal of Materials Chemistry B*, 2013, **1**, 4406-4418.

Table of Contents Graphic

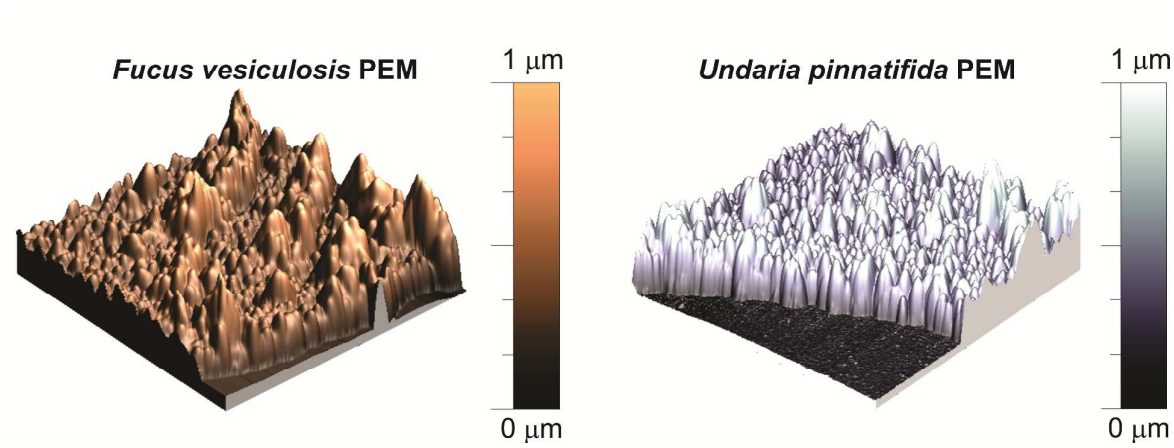

Polyelectrolyte multilayers of fucoidan with chitosan have film characteristics that depend on the species of seaweed from with the fucoidan is extracted. Acetylation of the fucoidan (and altered molecular weight) is implicated in the formation of denser, less hydrated multilayers.